

## Synthesizing 3-D Images with Voxels

Min-Chul Park, Sang Ju Park, Vladmir V. Saveljev,  
and Shin Hwan Kim

### 11.1 Introduction

3-D images provide viewers with more accurate and realistic information than 2-D images. They also bring immersive feeling to the viewers with depth sense, on the other hand, often causing dizziness and serious eye fatigue. The main demands of 3-D images occur in medical applications, advertisement, telepresence, education and entertainment, and so on.

Generally 3-D images adopt “voxel” representation, which is analogous to the concept of “pixel” in 2-D images. The voxels, basic elements of 3-D images, are used to describe virtual points. Any desired 3-D image can be displayed by synthesizing it with voxels of pre-defined coordinate values because 3-D images are formed by voxels. Voxels can be visible if a group of pixels in the display panel, which is responsible for making each voxel visible at the viewing zone, is defined because voxels are virtual points in a pre-defined space. The viewing zone is a spatial location where viewers can see entire images displayed on the screen.

The multi-view (MV) [1, 2, 3, 4, 5, 6, 7, 8, 9, 10, 11, 12, 13, 14] and IP (Integral Photography) [15, 16, 17, 18, 19, 20, 21, 22, 23] are the typical methods of displaying a full parallax 3-D image on a flat panel display. As autostereoscopic image displays these methods have been a matter of great concern since 1990. MV and IP have the same optical structure composed of a viewing zone forming optics and a display panel located at the focal plane

---

M.-C. Park

Intelligent System Research Division, Korea Institute of Science and Technology,  
Seoul, South Korea  
e-mail: minchul@kist.re.kr

of the optics. The images projected to viewers' eyes in MV and IP have a conjugate relationship between them [16]. In this chapter, synthesizing 3-D images with voxels in a contact-type imaging system for these methods will be discussed.

MV images for generating full parallax images can be easily obtained by using a two-dimensional (2-D) camera array. The images can also be synthesized with a computer by considering the relative viewing direction of each camera in the array for a given object [5, 6, 7, 12, 13, 14]. In order to configure these MV images, the display panels of MV 3-D imaging systems must be divided into a number of segments, called pixel cells. A 3-D imaging system can provide full parallax 3-D images.

Pixel cells (the number of segments divided) corresponds either to (1) the number of pixels in the image from each camera in the array [8, 9] or (2) to the number of cameras in the array [10, 11, 15, 16]. The number of pixels in each pixel cell is equal to the number of cameras in the array. Each pixel in the cell represents a pixel from each camera for (1). For (2), each pixel cell in the display panel presents the whole image of each camera. The each camera position in the array corresponds to that of the cell in the panel. The typical shape of a pixel cell is either rectangular or square. Since these shapes are vulnerable to the Moire effect, rhomb shaped pixel cells can also be used [24]. In these configuration methods, we typically scale the proper resolution of each camera image to fit into the resolution of the display panels available. This scaling process is somewhat cumbersome and time consuming.

3-D images are formed by voxels, so we can synthesize the 3-D image with voxels of pre-defined coordinate values [16, 25]. Finally, we can display any desired 3-D image. The voxels are used to describe virtual points. Any desired 3-D image can be displayed by synthesizing it with voxels of pre-defined coordinate values because 3-D images are formed by voxels. Voxels can be visible if a group of pixels in the display panel, which is responsible for making each voxel visible at the viewing zone, is defined because voxels are virtual points in a pre-defined space. The scaling step can be eliminated and the computational time for preparing MV images can be minimized. To obtain these effects a set of voxels is defined in the optical configuration of a full parallax MV 3-D imaging system based on a 2-D PLS (Point Light Source), and the set is used to display 3-D images.

In this configuration, the group of pixels provides passage for rays from PLSs such that the voxel is visible at the viewing zone's cross section, where the viewing zone is centered. The pixel pattern formed by the group of pixels has a unique pattern to represent a voxel in a certain location. Finding pixel patterns in the display panel is required so that it will be able to display 3-D images. The configuration provides two voxel types; one is seen at the entire viewing zone's cross section (complete voxel) and the other is only partially seen (incomplete voxel). The spatial volume is where 3-D images appear, and it depends on the spatial distribution of voxels. Similarly, the resolution of the images depends on their available number. As the number of complete

voxels is limited and the voxels occupy only a small space, the image space and the voxel resolution of the displayable images will be extremely limited as well. Using incomplete voxels will effectively increase the volume and the resolution of the images. The incomplete voxels will successfully increase the image volume in the MV 3-D imaging systems, since most of these systems [9, 10, 11] are based on the optical configuration [26].

The pixel patterns for these voxels strongly depend on the shape of the pixel cells. The pixel pattern for the complete voxel has the same pixel arrangement in both vertical and horizontal directions. For this reason, we are easily able to determine the 2-D pixel pattern from the vertical or horizontal direction pattern for a rectangular or square pixel cell. However, for the rhomb shaped pixel cell, the difference in pixel numbers in both directions changes the arrangements of directions from each other.

This chapter outlines synthesizing 3-D images with voxels in a contact-type imaging system by describing voxels in the PLS array and defining the incomplete voxels and their corresponding pixel patterns to increase the volume. Also, we mathematically identify their positions. In addition, we extend the pixel pattern to pixel cells with a rhombus shape for a Moire-free image display.

## 11.2 Description of Voxels in the Point Light Source Array

The central viewing zone forms the geometry of a 3-D imaging system. The 3-D image system is based on a PLS array shown in Fig. 11.1 that has the same number of PLSs in both horizontal and vertical directions. The PLSs are all in the same plane with an equal separation in all directions. A display panel is located in front of the PLS plane. The panel is divided into segments called pixel cells. Each segment that consists of pixel cells has an equal area and shape. These cells are arranged for full parallax image generation. They are the units of the MV images. Each cell is illuminated by its corresponding PLS. Therefore, the total number of cells in the panel is equal to the number of PLSs. The general shape of a cell is rectangular or square. Since each PLS illuminates the image display panel in front of it, all PLSs in the array should be shown at the viewing zone's cross section through the panel without any mismatch. All the magnified pixel cell images are superposed in the viewing zone. The viewing zone is the spatial region where viewers can observe 3-D images from the MV images on the panel.

Figure 11.2 shows the voxels and the voxel space defined in Fig. 11.1. The voxels are defined as the crossover points. These crossover points make the connection lines from each PLS to the four corners of the viewing zone's cross section.

This means: (1) each voxel is created by rays from four distinct PLSs in order to form the same shape as the viewing zone's cross section; (2) each

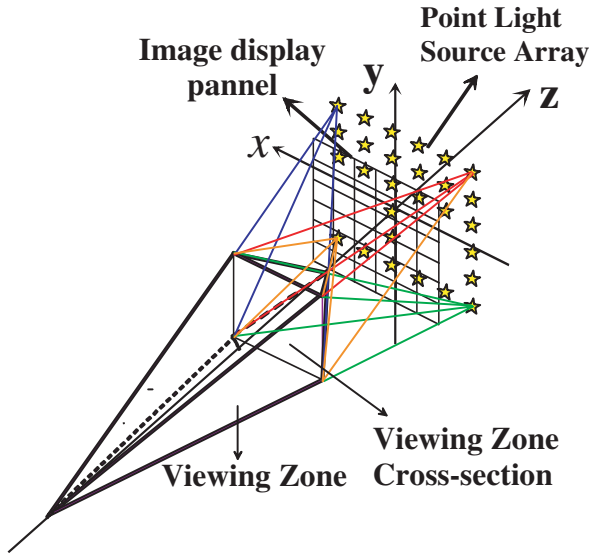


Fig. 11.1. Geometry of the viewing zone of a contact-type full parallax imaging system based on a PLS array

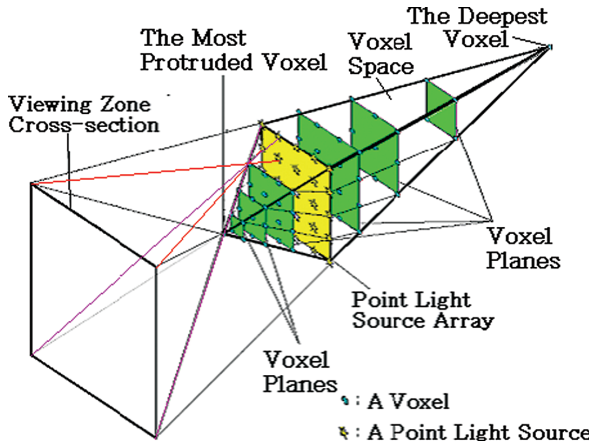


Fig. 11.2. Voxels and voxel space defined by the geometry of Fig. 11.1

voxel can be displayed at any location in the viewing zone's cross section, and (3) each voxel can be placed in a specific plane.

We define the pixel pattern for each voxel in the capacity of a portion of pixel cell through the PLS. The PLS corresponding to the cell can be seen at the cross section. The voxel space where the voxels are located is defined as a volume. The volume has a diamond shape because the synthesizable 3-D images with these voxels can exist only in a diamond shaped voxel space.

$M_S$  and  $N_S$  represent the numbers of PLSs in horizontal and vertical directions, respectively.  $N_T$  is the total number of voxels in the voxel space. When  $N_S > M_S$  as shown in Fig. 11.2,  $N_T$  is calculated as

$$N_T = \frac{M_S(3N_S M_S - M_S^2 + 1)}{3}. \tag{11.1}$$

When  $N_S < M_S$ ,  $N_S$  and  $M_S$  in Eq. (11.1) will be transposed. For the case when  $N_S = M_S$ , Eq. (11.1) can be simplified as,

$$N_T = \frac{M_S(2M_S^2 + 1)}{3}. \tag{11.2}$$

Figure 11.3 shows the top (horizontal plane) and side (vertical plane) views of the geometry in Fig. 11.2. This figure specifies the definition of complete and incomplete voxels for 6 X 6 PLS array. In this figure, voxels are described as the points dotted from PLSs to two edges of the viewing zone's cross section. This series of points (voxels) comprises the crossover lines in-between (between PLSs and two edges). Voxels are represented as squares for the first type and circles for the second type. The area with the incomplete voxels is much greater

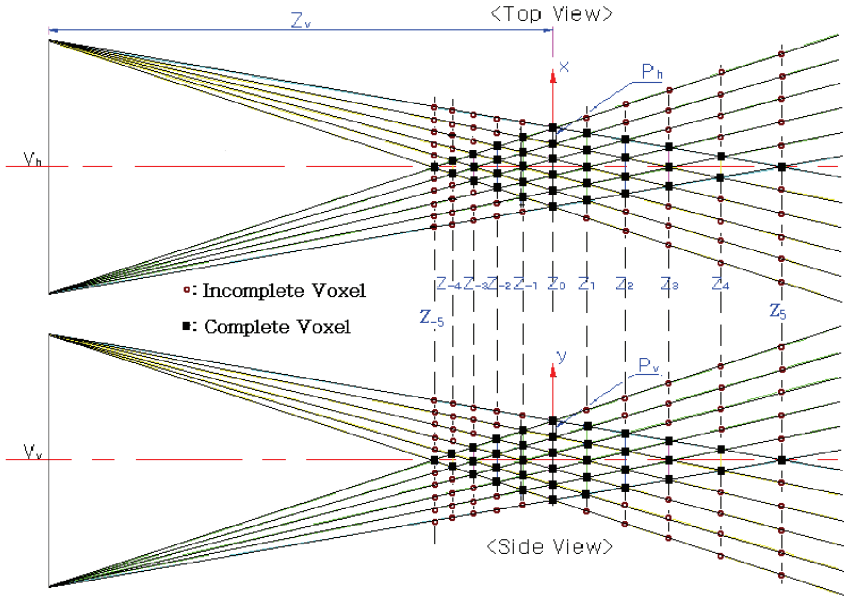


Fig. 11.3. Plane view of Fig. 11.2 defining complete and incomplete voxels

than that with complete voxels. This means that the voxel volume created by the incomplete voxels is much greater than the voxel space in Fig. 11.2.

From Fig. 11.3, the positions of the voxel planes in reference to the PLS array plane, which is located at  $z = 0$ , are calculated as,

$$z_k = |z_v| \frac{kP_h}{V_h - kP_h}, \quad z_k = |z_v| \frac{kP_v}{V_v - kP_v}. \tag{11.3}$$

$z_k$  and  $z_v$  represent the locations of  $k_{th}$  voxel plane and the viewing zone cross section, respectively.  $P$  is the end of PLSs and it can be expressed as  $P_h$  in the horizontal direction and  $P_v$  in the vertical direction.  $V$  is the size of the viewing zone's cross section, and it also can be expressed as  $V_h$  and  $V_v$  in horizontal and vertical directions, respectively.  $k$  is the order of voxel planes and has values  $k = 0, \pm 1, \pm 2, \pm 3, \pm 4, \dots, \pm M_S - 1$  and  $k = 0, \pm 1, \pm 2, \pm 3, \pm 4, \dots, \pm N_S - 1$ , where  $M_S$  and  $N_S$  represent the numbers of PLSs in horizontal and vertical directions, respectively. One can obtain the maximum value of  $k$  for the full parallax voxels taking the smaller value of  $|M_S|$  and  $|N_S|$ . In Eq. 11.3,  $z_k$  is not defined when  $V_h - kP_h \leq 0$  or  $V_v - kP_v \leq 0$ . In the coordinate defined in Fig. 11.3,  $k = 0$  and  $-1$  represents the plane of PLS array and the image display panel, respectively.  $Z_v$  has a negative value. If  $V_h/P_h = V_v/P_v = s$ , then  $z_k = k|z_v|/(s - k)$ , i.e.,  $z_k$  is just a function of  $k$ . This means that  $z_k$  has the same values in both horizontal and vertical directions.

The distance between voxels in the  $k_{th}$  plane,  $G_h^k$  and  $G_v^k$  ( $h$  and  $v$  represent horizontal and vertical directions, respectively) is calculated as,

$$G_h^k = \frac{V_h P_h}{V_h - k P_h}, \quad G_v^k = \frac{V_v P_v}{V_v - k P_v}. \tag{11.4}$$

The number of voxels in  $k_{th}$  plane is  $(M_S - |k|)(N_S - |k|)$  and the relative positions of voxels in  $k_{th}$  and  $(k + 1)_{st}$  planes are different. They are different about one-half voxel distance to each other in both horizontal and vertical directions. The difference is approximately half of the distance between two neighboring voxels in each plane in both the horizontal and vertical directions.

From Eq. (11.4), if  $i$  and  $j$  represent the order of voxels in horizontal and vertical directions from the  $z$  axis, respectively, the coordinate of each voxel in the  $k_{th}$  plane,  $X_k^{ij}(C_k^i, C_k^j, z_k)$ , are defined as,

$$C_k^i = iG_h^k \quad \text{and} \quad C_k^j = jG_v^k. \tag{11.5}$$

For

$$\begin{aligned} j &= 0, \pm 1, \dots, \pm \left( \left\lfloor \frac{N_S + 1 - |k|}{2} \right\rfloor - 1 \right) \\ i &= 0, \pm 1, \dots, \pm \left( \left\lfloor \frac{M_S + 1 - |k|}{2} \right\rfloor - 1 \right) \end{aligned} \quad (11.5a)$$

when

$$\left( \frac{N_S + 1 - |k|}{2} - \left\lfloor \frac{N_S + 1 - |k|}{2} \right\rfloor \right) = \left( \frac{M_S + 1 - |k|}{2} - \left\lfloor \frac{M_S + 1 - |k|}{2} \right\rfloor \right) = 0. \quad (11.5b)$$

Also,

$$\begin{aligned} C_k^j &= \frac{j}{2|j|} G_v^k + (j \mp 1) G_v^k (- : j > 0, + : j < 0), \\ C_k^i &= \frac{i}{2|i|} G_h^k + (i \mp 1) G_h^k (- : i > 0, + : i < 0), \end{aligned} \quad (11.6)$$

$$\begin{aligned} j &= \pm 1, \dots, \pm \left\lfloor \frac{N_S - |k|}{2} \right\rfloor, \\ j(i) &= \pm 1, \dots, \pm \left\lfloor \frac{M_S - |k|}{2} \right\rfloor \end{aligned} \quad (11.6a)$$

when

$$\left( \frac{N_S + 1 - |k|}{2} - \left\lfloor \frac{N_S + 1 - |k|}{2} \right\rfloor \right) = \left( \frac{M_S + 1 - |k|}{2} - \left\lfloor \frac{M_S + 1 - |k|}{2} \right\rfloor \right) = \frac{1}{2}. \quad (11.6b)$$

In Eqs. (11.5) and (11.6),  $i$  and  $j$  are 0 when voxels are on the horizontal and vertical planes, respectively. Both  $i$  and  $j$  have positive values if the voxels are in the first quadratic plane when they are seen from the VZCS (Viewing Zone's Cross Section), and  $\lfloor \cdot \rfloor$  sign denotes integer values. The conditions specified in Eqs. (11.5a) and (11.6b) are for odd and even values of  $N_S - |k|$  and  $M_S - |k|$ , respectively.

The voxels defined in Eqs. (11.1) and (11.2) represent those that have the pixel patterns shown in Fig. 11.4. Figure 11.4(a) comprises ray diagrams that define pixel patterns for voxels specified as squares in Fig. 11.3. The voxels are identified as  $X_k^i$  where  $i$  and  $k$  are the values defined above. In the instance of voxels  $X_{-2}^1$  and  $X_2^1$ , light sources 2, 3, and 4 can make these voxels visible at the viewing zone's cross section. Voxel  $X_{-2}^1(X_2^1)$  is visible at the bottom (top), middle and top (bottom) thirds of the viewing zone's cross section by the rays explained below. From light source 2, rays pass through the bottom (top) third of pixel cell 2 (from the top); from light source 3, rays pass through

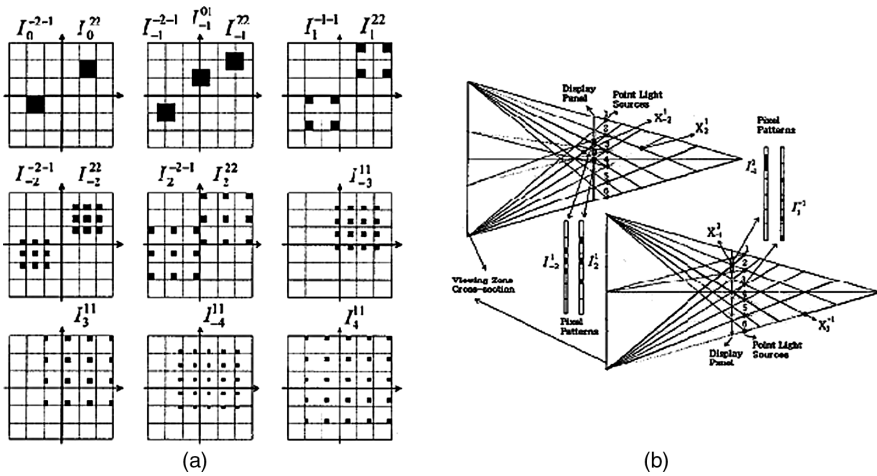


Fig. 11.4 (a) Ray diagram defining pixel patterns for voxels. (b) 2-D pixel patterns for the complete voxels defined in Fig. 11.3

the mid third of pixel cell 3 and, finally, from light source 4, rays pass through the top (bottom) third of pixel cell 4. Voxel  $X_{-2}^{-1}$  is visible at the bottom and top halves of the viewing zone's cross section by the rays explained below. From light source 1, rays pass through the bottom half of pixel cell 1, and from light source 2, rays pass through the top half of pixel cell 2. In the same way, voxel  $X_3^{-1}$  is visible at the top fourth, the second fourth, the third fourth, and the bottom fourth of the viewing zone's cross section, respectively, by the rays. These rays from light sources 3, 4, 5 and 6 pass through the top fourth of pixel cell 3, the second fourth of pixel cell 4, the third fourth of pixel cell 5, and the bottom fourth of pixel cell 6, respectively.

These rays eventually make the voxel visible at the top fourth, the second fourth, the third fourth, and the bottom fourth of the viewing zone's cross section, respectively. The one-dimensional pixel patterns for voxels  $X_{-1}^2$ ,  $X_{-2}^{-1}$ ,  $X_2^1$ , and  $X_3^{-1}$  and for voxels  $I_{-1}^2$ ,  $X_{-2}^{-1}$ ,  $I_2^1$ , and  $I_3^{-1}$  are shown in Fig. 11.4(a).

The pixel patterns obtained here reveal one serious problem related to this voxel method. We have made two assumptions about obtaining the patterns that have been explained above. The first is that the voxels in different  $k$  planes divide the viewing zone's cross section into  $k + 1$  different segments. A second assumption is that each segment is illuminated by its corresponding PLS. Based on these two assumptions of the patterns, the viewer's eyes should be positioned in the two different segments to understand the sense of depth with a specific voxel. Thus, the viewer would not be able to perceive the voxel to have a certain depth, if the widths or the segments are bigger than one's interocular distance. This problem applies to voxels in smaller  $|k|$  values. The solution to this problem is to reduce the width of the viewing zone's cross

section and to watch the images at a short distance from the display panel. A solution is to create 3-D images without using the voxels in the smaller  $|k|$  value plane; but in this case,  $|k|$  should be large enough. Figure 11.4(b) shows the 2-D extension of the patterns in Fig. 11.4(a). In this case the voxels and their pixel patterns are identified as  $X_k^{ij}$  and  $I_k^{ij}$ , respectively. It is shown that a pixel cell is divided into  $(|k| + 1)^2$ , and  $(|k| + 1)^2$  is equal segments for voxels in a  $k$ th plane.  $I_k^{ij}$  is composed of a segment from each  $(|k| + 1)^2$  neighboring to pixel cells.  $I_k^{ij}$  is a pattern with two-fold symmetry. The total area is occupied by these  $(|k| + 1)^2$  segments. This area is equal to the area of a pixel cell. Each pixel cell pattern corresponds to a complete voxel and the area occupied by the pattern (each pixel cell pattern) is equal to that of a pixel cell. The distance between the segments that compose the pixel pattern, in the unit of number of segments, is  $|k| \pm 1$ . The minus sign is for negative values of  $k$ . The voxels in the  $k_{th}$  plane are seen by each one of  $(|k| + 1)^2$  PLSs. Therefore, only two PLSs at a time can be seen by the viewer's two eyes.

### 11.3 Pixel Patterns of Incomplete Voxels

As Figs. 11.2, 11.3 and 11.4 show, each voxel in the voxel space has its corresponding pixel pattern in the display panel and, through the pixel pattern, it can be seen in any place in the viewing zone's cross section. If the patterns in the boundary of the panel are shifted one pixel cell at a time in each of four directions, (i.e., up-down and left-right), they become incomplete patterns and their corresponding voxels will be seen only at a specific part of the cross section. In Fig. 11.5, the patterns created shift the boundary pattern toward the right or the upper direction or both. Voxels that correspond to these patterns are called incomplete voxels and are marked as circles in Fig. 11.3.

These voxels are located at the crossover points of the extended row and column lines of the voxels in the  $k_{th}$  plane, and also on the lines drawn from each PLS to the four corners of the viewing zone's cross section. When these incomplete voxels are included, the voxel space has the shape of two trapezoidal pyramids sharing the PLS array's plane as their top sides. The height of the shape can be defined from the most protruding (outermost) voxel to the most submerged voxel.

The distances between incomplete voxels in the  $k_{th}$  plane are the same as those in the voxel space. As the pixel patterns for the voxels in the  $k_{th}$  plane are composed of  $|k| + 1$  pixel cells in each direction, they can be shifted  $k$  times in each direction. This means that, in the  $k_{th}$  plane, there are  $2|k|$  incomplete voxels in both the horizontal and vertical directions. The positions of the incomplete voxels can also be defined by Eqs. (11.5) and (11.6), but, in this case, the  $j$  and  $i$  values should be redefined as

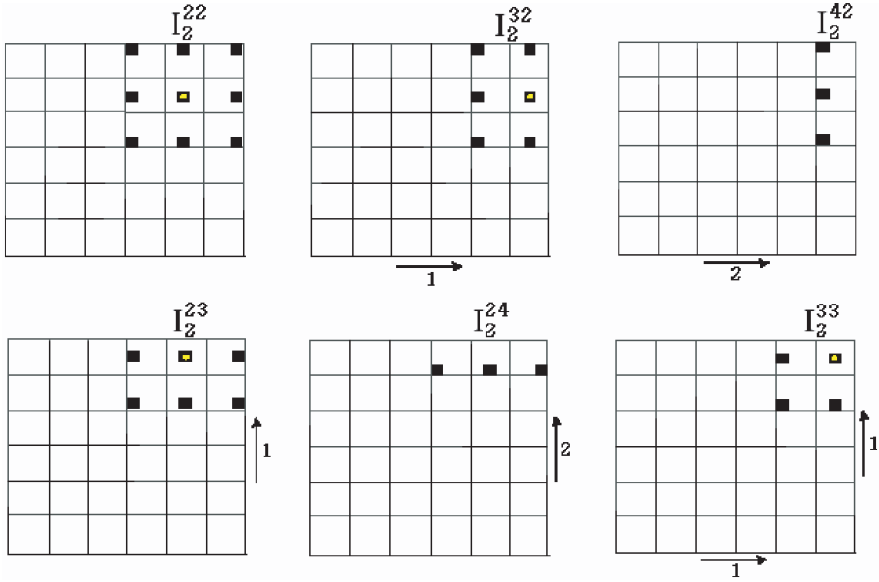


**Fig. 11.5.** Incomplete pixel patterns created by shifting the complete pixel pattern toward the right or upper direction or both

$$\begin{aligned}
 j &= 0, \pm 1, \dots, \pm \left( \left\lfloor \frac{N_S + 1 + |k|}{2} \right\rfloor - 1 \right), \\
 i &= 0, \pm 1, \dots, \pm \left( \left\lfloor \frac{M_S + 1 + |k|}{2} \right\rfloor - 1 \right)
 \end{aligned} \tag{11.7a}$$

for

$$\begin{aligned}
 \left( \frac{N_S + 1 - |k|}{2} - \left\lfloor \frac{N_S + 1 - |k|}{2} \right\rfloor \right) &= \left( \frac{M_S + 1 - |k|}{2} - \left\lfloor \frac{M_S + 1 - |k|}{2} \right\rfloor \right) = 0, \\
 j &= \pm 1, \dots, \pm \left( \left\lfloor \frac{N_S + |k|}{2} \right\rfloor \right), \\
 i &= \pm 1, \dots, \pm \left( \left\lfloor \frac{M_S + |k|}{2} \right\rfloor \right)
 \end{aligned} \tag{11.7b}$$

for

$$\left( \frac{N_S + 1 - |k|}{2} - \left\lfloor \frac{N_S + 1 - |k|}{2} \right\rfloor \right) = \left( \frac{M_S + 1 - |k|}{2} - \left\lfloor \frac{M_S + 1 - |k|}{2} \right\rfloor \right) = \frac{1}{2}.$$

In Eq. (11.7), the incomplete voxels are represented by  $j$  and  $i$  values bigger than those defined in Eqs. (11.5a) and (11.6a). With Eqs. (11.7) the total number of voxels, including the incomplete voxels,  $N_I$ , are calculated as

$$\begin{aligned}
N_I &= 2 \sum_{K=1}^{M_S-1} (N_S + K)(M_S + K) + N_S M_S \\
&= 2 \sum_{K=1}^{M_S-1} \{N_S M_S + K(M_S + N_S) + K^2\} + N_S M_S, \\
N_I &= \frac{M_S(5M_S^2 + 9N_S M_S - 6M_S - 6N_S + 1)}{3}.
\end{aligned} \tag{11.8}$$

For Eqs. (11.8) it is assumed that  $N_S > M_S$ . Because of the total number of incomplete voxels,  $N_{IV}$  equals to  $N_I - N_T$ , it is calculated from Eqs. (11.1) and (11.8) as,

$$N_{IV} = 2M_S(N_S + M_S)(M_S - 1) \tag{11.9}$$

When  $N_S = M_S$ , Eq. (11.9) can be rewritten as,

$$N_{IV} = 4M_S^2(M_S - 1) \tag{11.10}$$

A comparison of Eqs. (11.2) and (11.10) verifies that the number of incomplete voxels is  $\sim 6$  times greater than that of complete voxels. This means that the image space and voxel resolution will be increased  $\sim 7$  times greater than those with complete voxels only. The viewers can see the incomplete voxels in the parts of the viewing zone's cross section shown in Fig. 11.6.

There are 15 incomplete voxels: 5, 4, 3, 2 and 1 voxels on the lines connecting PLSs a, b, c, d, and e to the upper end of the viewing zone's cross section, respectively. The outermost incomplete voxels, numbered 1–5, are seen only at section A by PLS a. A is the uppermost section in six and it is equally divided viewing zone cross sections. Among the next four voxels numbered 6–9, voxels 6–9 are seen at sections D and F and at sections and E and F by PLSs f and e, respectively. These voxels are seen at two different segments. Accordingly, the inner voxels numbered 10–12, 13 and 14, and 15 are seen at three, four, and five sections, respectively. As the voxel arrangements in the upper and lower parts of Fig. 11.6 are symmetric along the  $z$  axis, the above analysis is valid for the voxels in both parts. There are another 15 incomplete voxels in the back side of the PLS array plane. These voxels can also be seen at parts of the viewing zone's cross section as their counterpart voxels in the front side of the array plane.

The incomplete pixel patterns look more like the pixel patterns in the voxel planes with smaller  $|k|$  values because the number of segments in the horizontal and vertical directions can be equal to each other. However, the differences in the relative position and size of each segment in each pixel cell, and the distances between neighboring segments, still distinguish the patterns. Using the incomplete voxels, we can remarkably increase the 3-D image space, compared with the complete-voxels-only case.

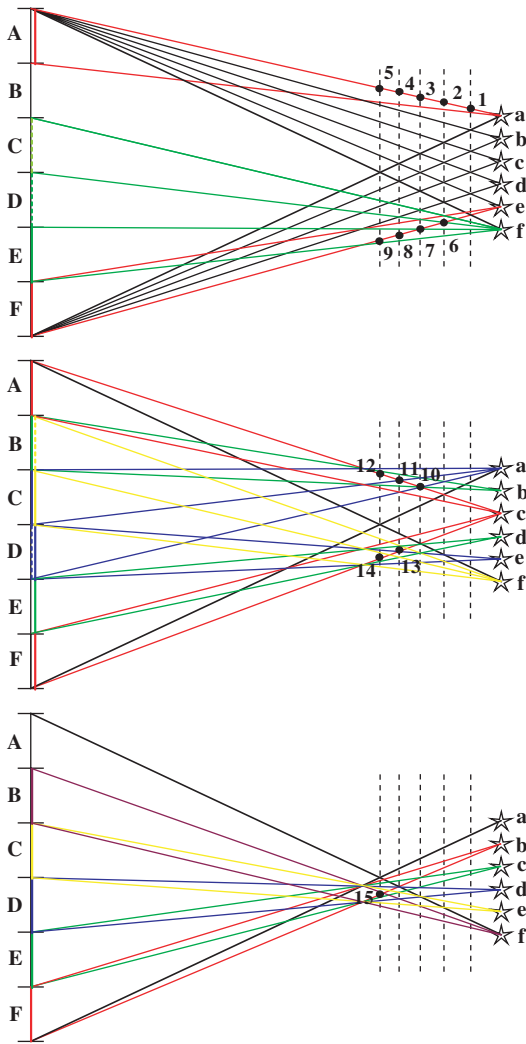
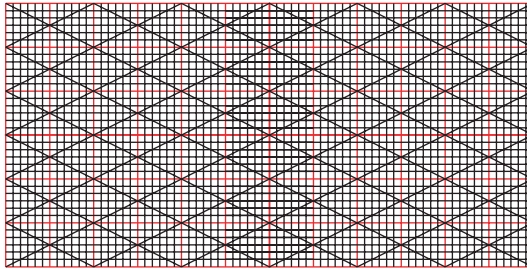


**Fig. 11.6** Parts of the viewing zone’s cross section where the incomplete voxels can be seen

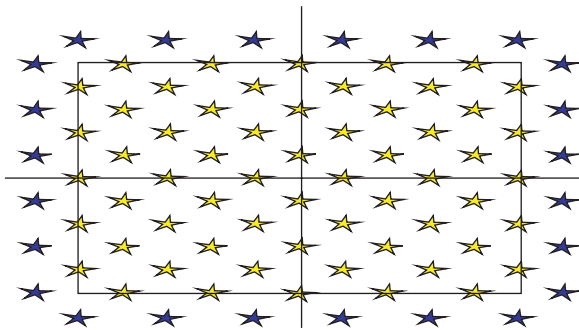
### 11.4 Pixel Patterns of Pixel Cells with Rhomb Shapes

To minimize the Moire effect rhomb shaped pixel cells have been used. The Moire effect occurs when overlaying optical plates to form a viewing zone on the display panel in a full parallax 3-D imaging system. There are two steps to create the rhomb cell. The first step is to overlay a rhomboidal net. A rhomboidal net consists of rhombs with a proper vertex angle onto a display

panel. The second step is to approximate the sides of each component rhomb. This process is necessary to discretize lines composed of boundaries of pixels along the sides. The net result of this operation is the same as rotating a square or rectangular pixel cell 45 degrees, and then squeezing or stretching the cell in either the horizontal or vertical direction to produce an appropriate vertex angle. Therefore, the pixel pattern for the rhomb shaped pixel cells will have the same pattern as that for the square or rectangular-shaped pixel cells rotated by 45 degrees. Figure 11.7 shows an image display panel with an arrangement of six rhomb shaped pixel cells in both the horizontal and vertical directions in Fig. 11.7(a). Its corresponding PLS array is shown in Fig. 11.7(b). The surface area of the display panel is divided into 72 equal rhombs. However, the total number of PLSs required to illuminate the panel is 84 because the edges of the panel are comprised of isosceles triangles with rhombic half-areas. Figure 11.8 shows voxel arrangements in voxel planes of  $|k| = 1$  in Fig. 11.8(a) and  $|k| = 2$  in Fig. 11.8(b). The voxel positions correspond to the four corner points of the pixel cells in the display panel in Fig. 11.7.



(a)



(b)

**Fig. 11.7.** Image display panel with an arrangement of six rhomb shaped pixel cells (a) in both horizontal and vertical directions, and (b) its corresponding PLS array

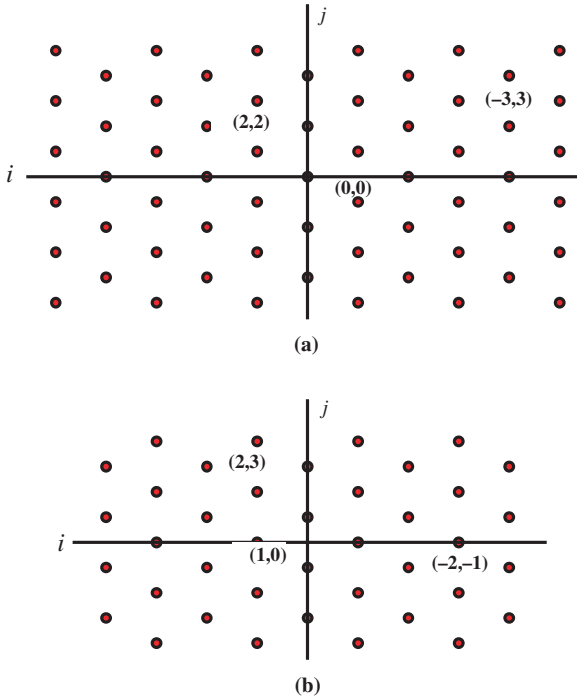


**Fig. 11.8.** Voxel arrangement in voxel planes of (a)  $k= 1$  and (b)  $k= 2$

In this arrangement, the coordinate of each voxel in the  $k_{th}$  plane,  $X_k^{ij}(C_k^i, C_k^j, z_k)$ , are defined as,

$$C_k^i = \frac{i}{2}G_h^k \quad \text{and} \quad C_k^j = \frac{j}{2}G_v^k \tag{11.11}$$

However, Eq. (11.11) is valid only for the following sets of  $i$  and  $j$  values: for  $i = 0, \pm 2, \pm 4, \dots, \pm(N_S - |k|)$ ,  $j = \pm 1, \pm 3, \pm 5, \dots, \pm(N_S - 1 - |k|)$  and for  $i = \pm 1, \pm 3, \pm 5, \dots, \pm(N_S - 1 - |k|)$ ,  $j = 0, \pm 2, \pm 4, \dots, \pm(M_S - |k|)$ , when  $N_S - |k|$  and  $M_S - |k|$  are even numbers. These sets of  $i$  and  $j$  values indicate that there are no voxels with  $i = \pm 1, \pm 3, \dots$  and  $j = \pm 1, \pm 3, \dots$ . When  $N_S - |k|$  or  $M_S - |k|$  are odd numbers, Eq. (11.11) will be satisfied for the following sets of  $i$  and  $j$  values:  $i = 0, \pm 2, \dots, \pm(N_S - 1 - |k|)$  and  $i = \pm 1, \pm 3, \dots, \pm(M_S - |k|)$ . These sets indicate that no voxels with even  $i$  and odd  $j$  values, or vice versa, exist.

A problem occurs with the pixel pattern for the rhomb shape. There is no 1:1 matching condition of pixels with rhomb shaped cells or segments, since the pixels are either square or rectangular. One can come up with two solutions to work out this problem: (1) any pixel in the rhomb is considered to

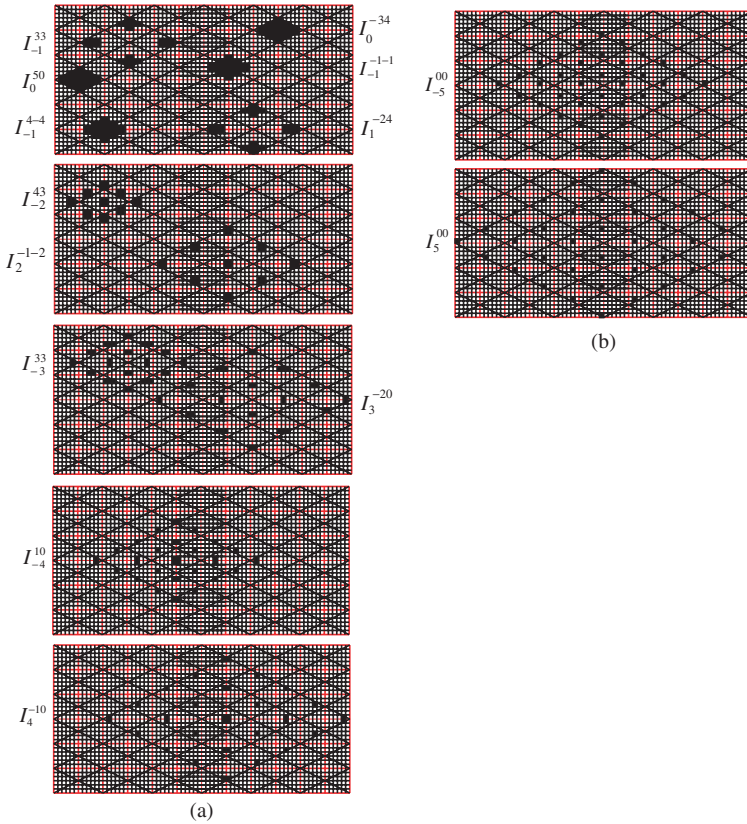


**Fig. 11.9.** Several pixel patterns for the voxels defined in Fig. 11.8

be in a rhomb or rhomb shaped segment if at least one-half of its area belongs to the rhomb, or (2) the total number of pixels should be close to the number in the rhomb. Figure 11.9 shows several pixel patterns for the voxels displayed in Fig. 11.8. The number of pixels in the patterns is 36. This is equal to the number of pixels in a rhomb cell.

Making use of the pixel patterns shown in Fig. 11.9, we are required to show the validity of the pixel patterns (Fig. 11.10). In order to show the validity, 3-D images of five different Platonic solids are generated on an LCD monitor with  $300 \mu\text{m}$  pixel size in both directions. Each of the solids is composed of pixel patterns. The pixel patterns correspond to  $\sim 150$  voxels scattered in nine different voxel planes ( $|k| = 4$ ). The solids reveal a good depth. But the images look discrete and change abruptly as the viewing direction changes. This is most likely so because the distances between voxel planes are longer than those between voxels in each voxel plane. Also some voxels in  $k = \pm 1$  and  $\pm 2$  planes do not appear in the 3-D sense because the designed width of

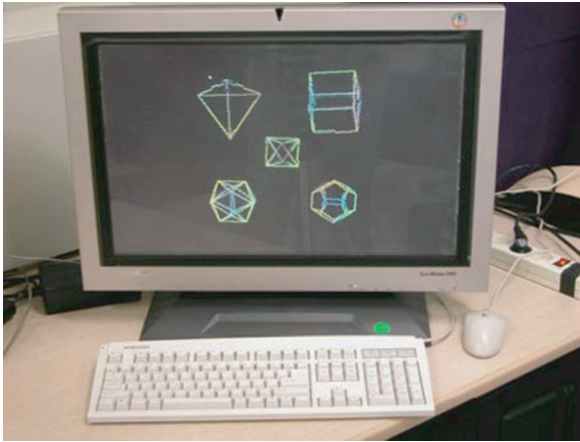


**Fig. 11.10.** 3-D images of five Platonic solids generated on a LCD monitor with  $300\ \mu\text{m}$  pixel in both directions

the viewing zone's cross section is 20 cm. In any case, Fig. 11.10 shows that the pixel patterns are valid. A magnified image of the combined pixel pattern on the LCD panel is shown in Fig. 11.11. This pattern is the pinnacle of an octahedron in the center of Fig. 11.10. It is encircled in the inset of Fig. 11.11. The rhomb shaped pixel pattern can be traceable from the pattern.

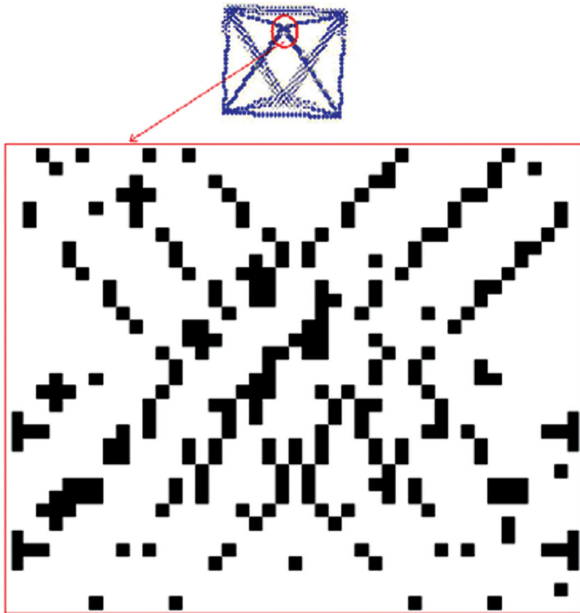


**Fig. 11.11.** Magnified image of the combined pixel pattern on the LCD display panel.

## 11.5 Comparison of 3-D Image Synthesis Between MV and IP Imaging Systems

The IP imaging system acquires and displays light rays passing through a plane. It has been regarded as one of the ideal 3-D photographic technologies. Integral imaging has the advantages of high 3-D luminance and full parallax, but has disadvantages of low 3-D resolution, Moire pattern, and color dispersion.

The MV and IP based on 3-D imaging methods practically have the same optical composition and structure, although the arranging methods of their MV image are different. The same optical structure causes the depth sense mechanism of both methods to be binocular parallax. On the other hand, the difference between them leads the projected images to be different view images [16]. These different view images are in the MV and are virtually synthesized images from the same number of pixels from all elemental images in the display panel.

In MV and IP, the image display panel is divided into pixel cells of an equal size and shape [4]. The pixel cell is located where MV images are arranged. It is the primary unit of display panel that presents MV images together. The viewing zone's cross section represents that all the magnified images of pixel cells by the corresponding lenslets are superposed. The viewing zone's cross section is parallel to the display panel. Pixel pattern in each pixel cell perfectly matches with those in other cells to a pixel unit.

When the viewing zone forms optics, it is said to be a special optical plate. The special optical plate is almost the same size as the panel. It consists of a 2-D array of elemental optics for full parallax image display. The array dimension is the same as the pixel cells in the panel. Various types of plates have been used as a role of optics, such as two superposed lenticular plates, a 2-D pinhole plate, a parallax barrier plate and a lenticular plate. The lenticular plate must be used with either a cross angle between them or 2-D microlens array plate. The lenslet is created by two superposed plates. The shape and size of each lenslet are the same as those of the pixel cells in the center of the panel. A 2-D PLS array can also be used as the optics. In this case it is located at the back side of the panel. We denote the horizontal length of the viewing zone's cross section, the distance between the viewing zone's cross section, and the microlens plate, as  $V_w$ .

Viewing distance and pitch of each lenslet (Pinhole, PLS) are denoted as  $a$  and  $P_L$ , respectively. Immediately the width of each pixel cell,  $C_w$  and focal length of the lenslet,  $f$  can be defined as,

$$C_w = \frac{P_L V_w}{V_w - P_L} \left( \frac{P_L V_w}{V_w + P_L} \text{ for PLS} \right) \quad \text{and} \quad f = \frac{a P_L}{V_w - P_L}, \quad (11.12)$$

respectively.

It is remarkable that the image depth can be maximized when these two conditions are satisfied. The parallax between left and right most viewing

images has to be smaller than interocular distance when the width of the viewing zone's cross section is made as close as the viewer's interocular distance.

Though current IP systems have a greater number of different view images than the MV, IP systems still provide a lower quality image than the MV. This is because the IP system, compared to MV, has the lower quality of resolutions in both recorded and synthesized images, and the effective size of its common viewing zone cross section is smaller. Therefore, it will be good to design IP's optical structure to satisfy Eq. (11.12) and to reduce the resolution of the recorded images for an improved image quality. This process can be done by minimizing the field of view angle of each lenslet. This improvement will accompany the increase in the total number of different view images, i.e., the total number of lenslets in the microlens plate [16].

## 11.6 Conclusion

Voxels are defined in the optical configuration of a full parallax MV imaging system based on a 2-D PLS array. The 3-D images synthesized by the voxels that have been described above, will be more spacious and refined with incomplete voxels. The voxels increase the image space and the image resolution up to  $\sim 7$  times greater than those with the complete voxels. We can assume that it is practicable to rotate a square shaped pixel cell 90 degrees. According to the procedure explained in this chapter, we can derive the pixel patterns for rhombic shaped pixel cells by rotating the pixel patterns for a square pixel cell 90 degrees, either clockwise or counterclockwise. The patterns permit images to be displayed with good 3-D quality, but the image quality can be improved. To improve the image quality, one should use the incomplete voxels effectively and use voxels in the higher  $|k|$  value planes. The MV and IP based on 3-D imaging methods practically have the same optical composition and structure, although the methods to arrange their MV image are different. To obtain an improved image quality in the IP system its optical structure should be designed to meet specific conditions described in Chapter 5, and reduce the resolution of the recorded images while increasing the total number of lenslets in the microlens plate.

## References

1. R. Borner: FKT. 45 (1991) 453
2. H. Isono, M. Yasuda and H. Sasazawa: 12th Int. Display Research Conf. Japan, Display'92 (1992) 303
3. T. Honda, Y. Kajiki, K. Susami, T. Hamaguchi, T. Endo, T. Hatada and T. Fuji: Three-Dimensional Television, Video, and Display Technologies. Ch. 19 (2002) 461

4. J. Y. Son, Ch. 2, in *Three-Dimensional Television, Video, and Display Technologies*, B. Javidi and F. Okano (eds.), Springer (2002)
5. L. F. Hodges and D. F. McAllister: "Computing Stereoscopic Views," in *Stereo Computer Graphics and Other True 3D Technologies*, D. F. McAllister (ed.), New Jersey, U.S.A.: Princeton University Press, Ch. 5 (1993) 71–89
6. K. Ji and S. Tsuji: *3 Dimensional Vision*, Tokyo, Japan, Kyoritz Publishing Company, Ch. 7 (1998) 95–110
7. Y. N. Gruts, J. Y. Son and D. H. Kang: "Stereoscopic Operators and Their Application," *J. Opt. Soc. Korea*, 5 (2002) pp 90–92
8. T. Izumi: *Fundamental of 3-D Imaging Technique*, NHK Science and Technology Lab., Tokyo, Japan: Ohmsa (1995)
9. J. Y. Son, V. V. Saveljev, Y. J. Choi, J. E. B. and H. H. Choi: "Parameters for Designing Autostereoscopic Imaging Systems Based on Lenticular, Parallax Barrier and IP Plates," *Opt. Eng.*, 42 (2003) 3326–3333
10. O. Matoba, T. Naughton, Y. Frauel, N. Bertaux and B. Javidi: "Real-time Three-dimensional Object Reconstruction Using a Phase-encoded Digital Hologram," *Appl. Opt.*, 41 (2002) 6187–6192
11. J. Ren, A. Aggoun and M. McCormick: "Computer Generation of Integral 3D Images with Maximum Effective Viewing," *SPIE Proc.* 5006 (2003) 65–73
12. J.-Y. Son, V. V. Saveljev, B. Javidi, D.-S. Kim and M.-C. Park: "Pixel Patterns for Voxels in a Contact-type 3-D Imaging System for Full-parallax Image Display," *Appl. Opt.*, 45(18) (2006) 4325–4333
13. J. Y. Son, B. Javidi and K. D. Kwack: *Proceedings of the IEEE, Special Issue on: 3-D Technologies for Imaging & Display.* 94(3), (2006) 502
14. J.-Y. Son, and B. Javidi: "3-Dimensional Imaging Systems based on Multiview Images," *IEEE/OSA J. Display Technol.* 1 (2005) 125–140
15. F. Okano, H. Hosino, J. Arai, M. Yamada and I. Yuyama: "Three Dimensional Television System Based on Integral Photography," in *Three-Dimensional Television, Video, and Display Technique*, B. Javidi and F. Okano (eds.) Berlin, Germany: Springer (2002)
16. J.-Y. Son, V. V. Saveljev, K.-T. Kim, M.-C. Park and S.-K. Kim: "Comparison of Perceived Images in Multiview and IP based 3-D Imaging Systems," *Jpn. J. Appl. Phys.*, 46(3A) (2007) 1057
17. F. Okano, H. Hoshino and I. Yuyama: *Appl. Opt.* 36 (1997) 1598
18. J.-S. Jang and B. Javidi: *Opt. Lett.* 28 (2003) 324
19. H. Liao, M. Iwahara, N. Hata, T. Dohi: *Opt. Exp.* 12 (2004) 1067
20. L. Erdmann and K. J. Gabriel: *Appl. Opt.* 40 (2001) 5592
21. H.E. Ives: *J. Opt. Soc. Am.* 21 (1931) 171
22. C. B. Burckhardt: *J. Opt. Soc. Am.* 58 (1967) 71
23. T. Okoshi: *3 Dimensional Imaging Techniques.* Ch 2 (1976) 21
24. I. Amidror: *The Theory of the Moire Phenomenon*, Kluwer Academic Publishers (2000)
25. J.-Y. Son and B. Javidi: "Synthesizing 3 Dimensional Images Based on Voxels," *SPIE Proc.* V5202 (2003) 1–11
26. A. Watt: *3D Computer Graphics*, 3rd Edition, Addison-Wesley, Harlow, England, Chap. 13 (2000) 370–391